A Robotic Ankle–Foot Prosthesis With Active Alignment

Andrew Kennedy LaPrè
Department of Mechanical and Industrial Engineering,
University of Massachusetts Amherst,
160 Governors Drive,
Amherst, MA 01003
e-mail: alapree@umass.edu

Brian R. Umberger
Department of Kinesiology,
University of Massachusetts Amherst,
30 Eastman Lane,
Amherst, MA 01003
e-mail: umberger@umass.edu

Frank C. Sup IV[1]
Department of Mechanical and Industrial Engineering,
University of Massachusetts Amherst,
160 Governors Drive,
Amherst, MA 01003
e-mail: sup@umass.edu

An ankle–foot prosthesis designed to mimic the missing physiological limb generates a large sagittal moment during push off which must be transferred to the residual limb through the socket connection. The large moment is correlated with high internal socket pressures that are often a source of discomfort for the person with amputation, limiting prosthesis use. In this paper, the concept of active alignment is developed. Active alignment realigns the affected residual limb toward the center of pressure (CoP) during stance. During gait, the prosthesis configuration changes to shorten the moment arm between the ground reaction force (GRF) and the residual limb. This reduces the peak moment transferred through the socket interface during late stance. A tethered robotic ankle prosthesis has been developed, and evaluation results are presented for active alignment during normal walking in a laboratory setting. Preliminary testing was performed with a subject without amputation walking with able-bodied adapters at a constant speed. The results show a 33% reduction in the peak resultant moment transferred at the socket limb interface.
[DOI: 10.1115/1.4032866]

Keywords: ankle prosthesis, transtibial amputation, gait, active alignment

1 Introduction

The performance of an individual with lower limb amputation is limited by a combination of their altered morphology, the prosthesis, and the connection between them. Current lower limb prostheses, both active and passive, are designed to recreate the biomechanics of intact limbs [1]. This mimic-type approach assumes that the socket connecting the wearer to their prosthesis is a perfect mirror of the intact limb. During walking, however, the prosthesis loads the residual limb at the socket interface, stressing the soft tissue of the limb. This can cause localized pain and tissue damage, as well as injury to the other parts of the musculoskeletal system as the person adapts to and compensates for the device. As a result, persons with lower limb amputation are at greater risk for osteoarthritis, osteopenia, osteoporosis, and back pain [2–5]. Decline in mobility due to discomfort and deterioration of overall health is common and leads to a more sedentary lifestyle [6]. This further compromises the person's health status through muscle atrophy, decreased bone density, and weight gain [5]. A lower limb prosthesis designed to decrease the loads placed on the residual limb has the potential to impact one's mobility in order to sustain a more active lifestyle, without creating health problems associated with high peak load conditions.

Motivated by both the form and function of the lost limb, the design of lower limb prostheses has historically been driven to restore individuals with amputation to a physiologically normal gait with intact limbs [1]. This includes factors such as size, mass, torque, speed, stiffness, range of motion, responsiveness to commands, and net-positive work ability of an intact limb [7–9]. Differences in physiology of intact and amputated limbs may limit the success of this approach. In an intact limb, the gastrocnemius and soleus muscles generate a majority of the sagittal moment about the ankle joint during push off. The gastrocnemius is biarticular and also acts to transfer energy from the knee to the ankle joint, contributing to whole body angular momentum [10–12]. Examining the paths of the intact gastrocnemius and soleus shows that these muscles counter the moment transferred through the tibia when a moment is generated about the ankle (Fig. 1(*a*)). In a limb that has been partially amputated, the bones and muscles are severed and the sagittal moment generated by the prosthesis is transferred at the socket–limb interface through the soft tissue to the bone. As a result of this nonrigid connection, unnatural compressive and shear loading of soft tissue occurs as well as irregular moment loading of bone tissues (Fig. 1(*b*)). In an evaluation of a commercial powered ankle–foot with healthy joint performance capabilities [7], the altered musculoskeletal anatomy of the affected limb combined with socket movement under loading may have contributed to a decrease in metabolic performance. This was attributed to the recruitment of additional muscles in comparison to healthy controls [13]. Further, it is observed that the GRF during push off with a powered ankle–foot compared to passive prosthetic feet shows little improvement, in terms of better resembling that of a person without amputation [14]. It is possible that the socket interface may be fundamentally limiting the effectiveness of a prosthesis, even if the prosthesis replicates the performance of an intact limb locally.

Different socket designs are used to load the residual limb with varying strategies. Load concentrating sockets such as the patellar tendon bearing socket focus the loads in the patellar tendon and

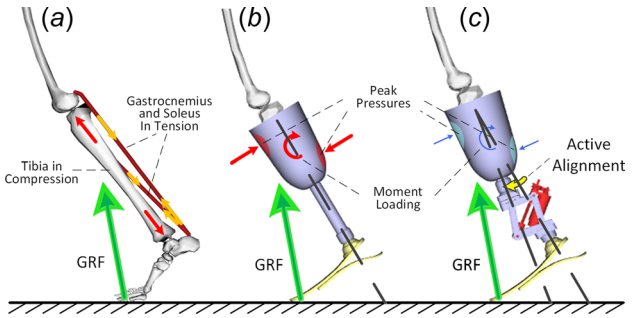

Fig. 1 The gastrocnemius and soleus muscles in a person with amputation generate a majority of the sagittal moment about the ankle, but also counter the moment transfer through bone tissue, keeping the tibia mostly in compression (*a*). High peak pressures are observed on the patellar tendon and distal posterior regions of the residual limb when using a conventional prosthesis as a result of high moment transfer through the socket interface (*b*). The active alignment prosthesis realigns the residual limb toward the CoP during midstance to reduce moment transfer while producing net-positive work (*c*).

[1]Corresponding author.

Manuscript received November 18, 2014; final manuscript received February 10, 2016; published online May 12, 2016. Assoc. Editor: Venketesh Dubey.

Fig. 2 Active alignment prosthesis tethered prototype shown with protective covers and foot shell. The prototype was developed to evaluate modified gait mechanics for reduced moment loading of the residual limb and restoration of rest of body biomechanics.

distal posterior regions of the residual limb [15–17] producing high cyclical peak pressures on tissues that have not evolved to tolerate such loading in a repetitive manner [18]. Other socket designs, such as total surface bearing (TSB) sockets, attempt to distribute the loads over the entirety of the residual limb to reduce peak pressures [19,20]. Even with distributing loading, pain, skin abrasions, and scarring due to high inner-socket pressures are still common issues. There have been reported cases where TSB sockets are not always a better option, typically when neuromas or exaggerated bone spurs are present [19,21].

Different methods are used clinically to reduce inner-socket peak pressures. A static alignment of the prosthetic foot to the posterior of the limb reduces the peak sagittal moment generated during push off [22]. This, however, increases the negative moment following heel strike (HS) and reduces the center of mass (CoM) height during roll over [8,11]. Compliance is often added to the socket with gel liners to distribute large forces [23], but it has been observed that thick liners reduce the sense of stability, sensory feedback, and efficiency in energy transfer with increased socket movement [24].

The primary contribution of this paper is a prosthesis design approach that reduces the moment loading at the socket–limb interface, while generating net-positive work. The goal is to complement the unique anatomy of a person with amputation rather than try to mimic the morphology and performance of the missing limb segment. Our preliminary biomechanical analyses and simulations have shown that near-normal whole body gait dynamics can be achieved while also lowering moment loading on the residual limb by actively realigning the limb with respect to the foot prosthesis during gait [25]. Active alignment allows for continuously varying the prosthesis–limb relative orientation throughout stance. It enables the residual limb to be nominally aligned with the foot during HS and anteriorly shifted at toe off (TO). This physically reduces the sagittal plane moment arm between the GRF at the CoP and the socket connection during late stance (Fig. 1(*c*)). The peak moment per GRF generated is reduced while smoothly transferring power from the prosthesis to the limb during midstance over a longer period of time, instead of in a sudden burst in late stance. During the realignment, the prosthesis concurrently lifts the body CoM for a more natural CoM trajectory, reducing the need for rest of body compensation commonly seen in gait post amputation.

This paper presents the design of an experimental, tethered robotic ankle prosthesis with active alignment. The mechatronic system is described including the sensing and control. Experimental results evaluating active alignment are performed using a bench top setup and walking experiments using able-bodied adapters. The performance, design advantages and disadvantages, and implications of the device on whole body biomechanics are discussed. Finally, conclusions and closing remarks about the potential design methodology and future works are made.

2 Methods

2.1 Design of Robotic Ankle Prosthesis With Active Alignment. An experimental tethered prosthesis prototype (Fig. 2) was developed for evaluation of active alignment in a lab environment. An optimized four-bar linkage was used to both rotate and translate the foot relative to the shank using a single actuator, as shown in Fig. 3. During midstance, the ball screw actuator develops a tensile force between the joint connecting posterior links and the joint connecting the anterior links. As the actuator contracts, the prosthesis extends and shifts the foot center

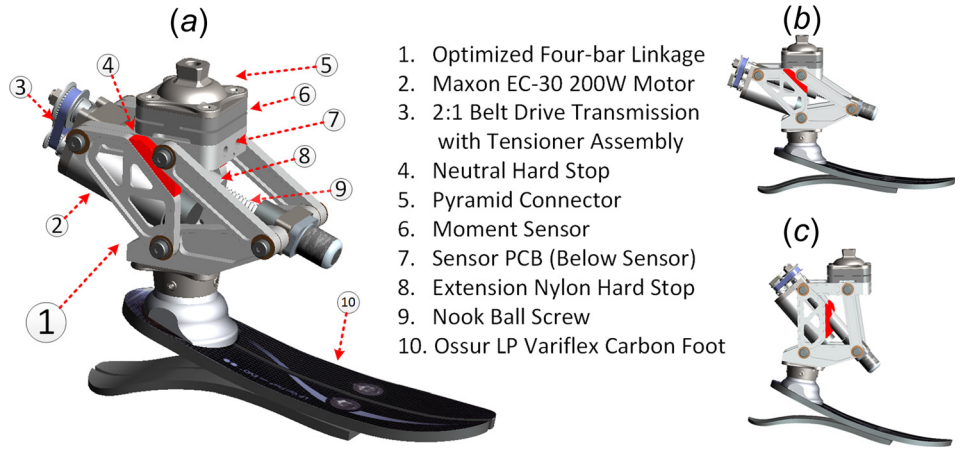

Fig. 3 Solid model of the active alignment prosthesis. The design is shown without covers, featuring major components (*a*). The prosthesis model is displayed in a neutral position (*b*) and fully extended (*c*) showing the modified kinematics.

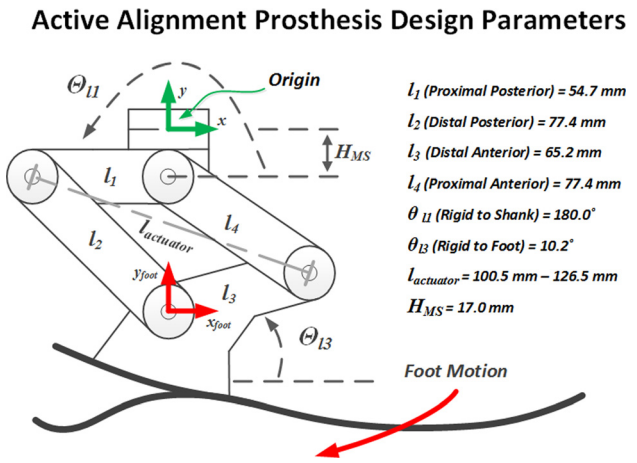

Fig. 4 Four-bar linkage design parameters with optimal values. The linkage motion directions x_{foot}, y_{foot}, and θ_{foot} are shown in the shank reference frame as commonly modeled in practice (proximal to distal). The foot motion can be calculated as a function of a variable linear actuator length and the given design parameters. The optimal link lengths given are the distances between joint centers on the links indicated in subscript. The optimal rigid attachment angles, of links 1 and 3 to the shank and foot, respectively, are given.

of rotation to align the residual limb anteriorly toward the CoP. Immediately following TO, the prosthesis quickly returns to a neutral alignment to provide ground clearance during swing.

The prosthesis linkage design parameters consist of link lengths (l_1, l_2, l_3, and l_4) and rigid attachment angles of link 1 to the shank and link 3 to the foot (θ_{l1} and θ_{l3}), as shown in Fig. 4. Optimal parameter values were found in Refs. [25] and [26] by analyzing recorded able-bodied kinematics and calculated kinematics from a model with a unilateral, transtibial amputation and the parameterized prosthesis concept, to minimize the prosthesis height with the following kinematic constraints:

(1) In the "neutral" position, the active alignment prosthesis was not extended and aligned the model (foot, knee center of rotation, and knee angle) with the able-bodied kinematic data in a standing posture. This constraint ensured that the prosthesis would perform as a conventional passive prosthesis when not being actuated.
(2) The center of rotation of the affected knee and hip was aligned with able-bodied kinematics at TO. This constraint was used to realign the rest of body to able-bodied kinematics.
(3) At TO, the knee and the prosthesis linkage were both fully extended. This constraint was implemented to create a maximum alignment range.
(4) Positive prosthesis extension always translated the foot prosthesis both posteriorly and distally relative to the socket and plantar flexed the foot. This constraint eliminated linkage configurations that would cause the foot to reverse linear or rotational directions to arrive at the correct final alignment during extension.

The assumptions of the model with amputation are as follows:

(1) The limb–socket connection was an ideal rigid joint.
(2) Joint dynamics of the rest of body (head, arms, torso, and unaffected leg) were restored to able-bodied values with the exception of affected limb stance knee flexion, CoP is unchanged from healthy data during walking, and the energy storage and return (ESAR) foot flexed an amount calculated by the foot stiffness, body weight, and CoP.

Prosthesis kinematic equations were derived, using the moment sensor, with height H_{MS} in relation to the joint connecting proximal links, as the origin. Equations (1)–(3) describe foot translations x_{foot}, y_{foot} and rotation θ_{foot} as functions of the design parameters and variable linear actuator length $l_{actuator}$, which is the distance between the joint connecting posterior links and the joint connecting the anterior links. Design parameters consisted of static link lengths (l_1, l_2, l_3, and l_4) and rigid connection angles of links 1 and 3 to the shank and foot (θ_{l1} and θ_{l3}), respectively. The foot translation was described using the motion of link 3 (fixed rigidly to the foot) with the joint connecting the two distal links as the local reference frame. These equations were used to solve for the ideal parameters with the kinematic constraints and assumptions given above. The actuator length was used as an input to attain the kinematics of the foot in relation to the residual limb with specified design parameters

$$x_{\text{foot}} = l_1 \cdot \cos(\theta_{l1}) + l_2 \cdot \cos\left\{\theta_{l1} - 180 - \cos^{-1}\left(\frac{l_1^2 - l_4^2 + l_{\text{actuator}}^2}{2 \cdot l_1 \cdot l_{\text{actuator}}}\right) - \cos^{-1}\left(\frac{l_2^2 - l_3^2 + l_{\text{actuator}}^2}{2 \cdot l_2 \cdot l_{\text{actuator}}}\right)\right\} \tag{1}$$

$$y_{\text{foot}} = -H_{\text{MS}} + l_1 \cdot \sin(\theta_{l1}) + l_2 \cdot \sin\left\{\theta_{l1} - 180 - \cos^{-1}\left(\frac{l_1^2 - l_4^2 + l_{\text{actuator}}^2}{2 \cdot l_1 \cdot l_{\text{actuator}}}\right) - \cos^{-1}\left(\frac{l_2^2 - l_3^2 + l_{\text{actuator}}^2}{2 \cdot l_2 \cdot l_{\text{actuator}}}\right)\right\} \tag{2}$$

$$\theta_{\text{foot}} = \theta_{l1} - \theta_{l3} - \cos^{-1}\left(\frac{l_1^2 - l_4^2 + l_{\text{actuator}}^2}{2 \cdot l_1 \cdot l_{\text{actuator}}}\right) - \cos^{-1}\left(\frac{l_2^2 - l_3^2 + l_{\text{actuator}}^2}{2 \cdot l_2 \cdot l_{\text{actuator}}}\right) - \cos^{-1}\left(\frac{l_2^2 + l_3^2 - l_{\text{actuator}}^2}{2 \cdot l_2 \cdot l_3}\right) \tag{3}$$

Predictive, forward dynamics simulations were performed in prior work to verify the design [25]. The simulations compared a model modified to reflect transtibial amputation to an intact model tracking able-bodied kinematics. In separate simulations, the modified model was connected to the concept prosthesis, a passive ESAR prosthesis, and an active biomimetic prosthesis for comparison. Simulation results showed that the CoM trajectory of the modified model when attached to the active biomimetic and concept prosthesis was comparable to that of the intact model, but diverged when attached to the passive prosthesis. The model

utilizing the concept prosthesis showed noteworthy reduction of moment transfer at the socket–limb interface in comparison to when attached to both passive ESAR foot prosthesis and active biomimetic prosthesis.

The prototype ankle–foot prosthesis was designed to be actuated by a brushless DC motor (EC-30, Maxon Motors, Sacheln, Switzerland) rated for 200 W at 5.0 A nominal current and can be driven up to 15 A peak current. The motor was coupled to a 2.5 mm lead 8 mm diameter ball screw (ECS-08025, Nook Industries, Cleveland, OH) with a 2:1 belt drive transmission for a peak linear actuator force of 1.87 kN. The ball screw was centered on opposing anterior and posterior rotational joints of the linkage with trunnion type mounts to prevent a bending moment. Current was supplied to the motor by a driver (ESCON 50/5, Maxon Motors) and supplied by a 40 V DC power supply. All the controls were performed in MATLAB/SIMULINK real-time workshop (MathWorks, Natick, MA), and communication to the driver and onboard sensors was done using a data acquisition (DAQ) card (PCI-6229, National Instruments, Austin, TX) with a 1000 Hz sample rate. All the analog signals were processed with a finite impulse response filter with pass and stop frequencies and amplitudes of 30 Hz and 50 Hz and 1 dB and 20 dB, respectively. Analog signals from onboard sensors were sent through a shielded cable which was grounded at the DAQ card and attached to the motor frame on the prosthesis end. The prosthesis was attached to an ESAR prosthetic foot (Ossur, Variflex LP). Neutral alignment hard stops made from urethane rubber with a shore stiffness of 80 (US Composites, POLY-75801) were molded into the lower posterior links to support the upper anterior links at neutral foot alignment. The stops provided support during standing, absorb shock load during HS, and limited dorsiflexion of the foot. An extension hard stop machined from nylon stock was placed around the ball screw between the posterior and anterior linkage joints to limit prosthesis extension. Geometry features of the prosthesis links were optimized for weight and a safety factor of two via feature parameterization and optimization using computer-aided design modeling (PTC Creo Parametric, Needham, MA) and finite-element analysis (ANSYS Workbench, Canonsburg, PA). Prosthesis links were machined from aluminum (AA-6061) and connected with shoulder bolts (grade 8) to the actuator bearing block and ball screw nut block. Needle bearings (QBC bearings) supported the shoulder bolts, and thrust washers were cut from phosphor bronze shim stock (LYON Industries) with thickness of 0.018 in. (0.46 mm) to separate the links and reduce friction. Three-dimensional printed protective covers (Stratasys, Rehovot, Israel) prevented insertion of foreign objects and appendages into mechanism pinch-points. All the remaining assembly hardware were stainless steel.

2.2 Sensing and Control. The prosthesis was controlled using position, inertial, and force data from onboard sensors as inputs to a finite state controller and a nested closed-loop controller. Safety was a primary concern during design and leads to control features built into both hardware and software for emergency stops, limits, and other features to prevent harm to the test subjects and operators.

To measure the socket moment, a low-profile moment sensor was positioned at the prosthesis–socket interface [27]. The sensor was designed to be insensitive to off-axis and direct loading for accurate moment sensing and to be compact and light-weight as not to add significant height or mass to the overall prosthesis design. Moment loads transmitted through the socket were captured to provide feedback to the controller (Fig. 5(*a*)). The sensor design was parameterized and optimized with finite-element analysis (ANSYS Workbench, Canonsburg, PA) to be strain-matched to the foil strain gages used (Vishay Micromeasurements) under maximum loading conditions (combined 120 N · m sagittal moment and 1200 N axial loading). The gages were oriented and wired to cancel out axial and off-axis loading. The signal from the bridge was amplified (gain: 99.8) and filtered (50 Hz cutoff frequency) on a custom-printed circuit board (PCB) (Fig. 5(*b*)) before being sent to the DAQ card (National Instruments, PCI-6229) via tether. Amplifier output had a 0.0–5.0 V range which could be manually zeroed with a precision tuning potentiometer for a desired load range offset. The custom PCB also integrated a two-axis gyroscope and three-axis accelerometer. The motor was controlled using a current controller built into the driver (Maxon Motors, ESCON 50/5). The driver was given a desired current command which was calculated by other closed-loop controllers for position, velocity, or moment control.

The controllers were implemented utilizing a proportional, integral, derivative (PID) feedback loop, which took the standard form of

$$I_M = K_P e + K_I \int e + K_D \dot{e} \tag{4}$$

where I_M was the current commanded to the motor driver, e was the error of the feedback being controlled, and K_P, K_I, and K_D were the scheduled proportional, integral, and derivative gain parameters. The gain parameters were estimated by using a model of the motor and linkage response utilizing the torque constant provided by the manufacturer to calculate prosthesis force output, taking into account the system mechanical advantage at the different amounts of prosthesis extension used in the benchtop testing. Further tuning was performed manually using the Zeigler–Nichols tuning method [28].

To ensure safety to the user and surrounding people during testing, redundant safety control mechanisms were included in the hardware, software, and experiment designs. Both the operator and subject had handheld tethered emergency stop switches that turn off power to the prosthesis in the case of a malfunction. There were emergency stops built into the architecture of the motor controller and in SIMULINK which stopped operation in the case when over current to the motor was sensed to prevent damage to the hardware.

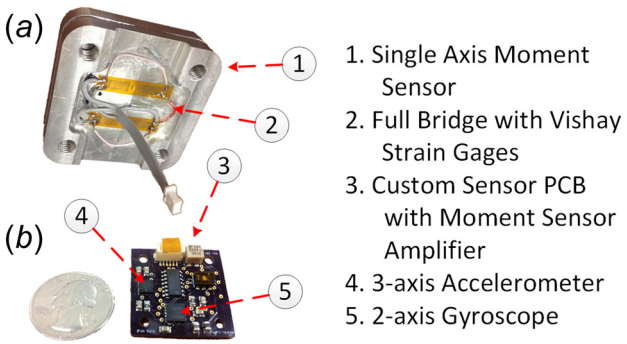

Fig. 5 The single axis moment sensor is shown with strain gages on the underside (*a*) and the custom sensor PCB (*b*), which amplifies the moment sensor signal and measures inertial dynamics

2.3 Device Characterization. Bench top characterization was performed to tune and demonstrate performance of the active alignment prosthesis. Moment sensor output and error were tested and calculated. Step response was recorded for force and power output, and frequency response was recorded to identify the controllable bandwidth.

To characterize the moment sensor, it was removed from the prosthesis and fixed to a rigid fixture by the base of the sensor (Fig. 6(*a*)). An arm was fastened to the top of the sensor in order to produce known moments by hanging known masses 0.250 m from the center of the sensor. Applied moments were loaded and unloaded between static measurements of the sensor output voltage to characterize the sensor from −50 to 100 N · m. Negative

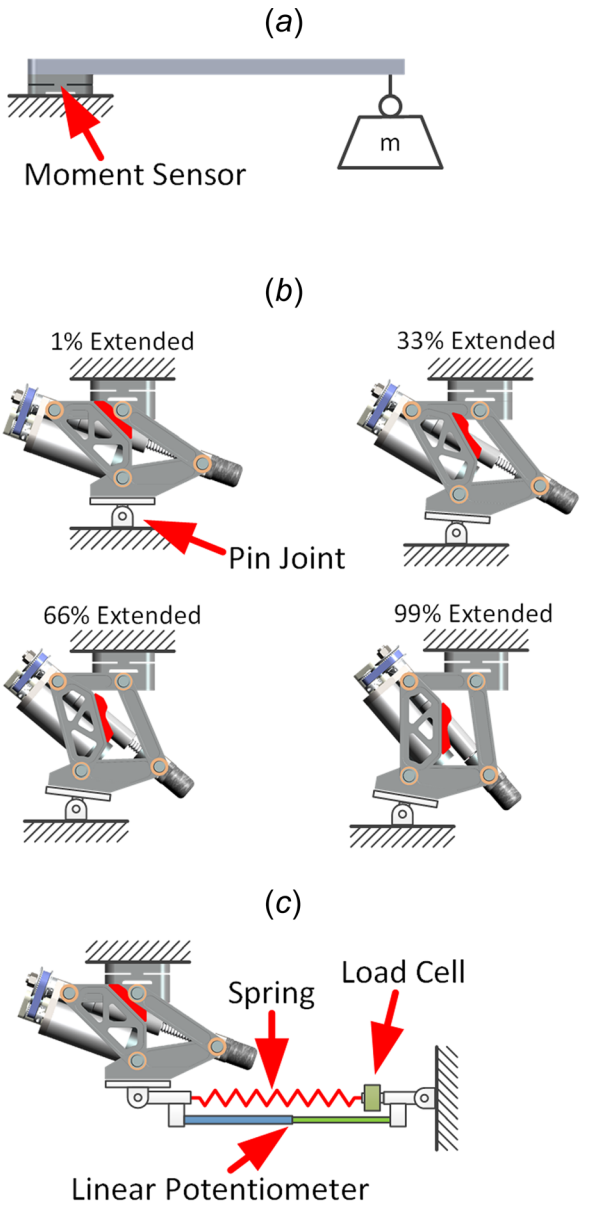

Fig. 6 Experimental setups used for characterization and initial testing. To characterize the moment sensor, the bottom was bolted to ground and a 0.25 m moment arm was attached to the top to apply known moments (*a*). For tuning and step/frequency responses, the prosthesis was mounted rigidly to ground by the moment sensor and pinned to ground at the foot connection for zero moment loading in four increments of extension (*b*). For power output testing, the prosthesis was mounted in a custom dynamometer that bolts the moment sensor to ground and pins the foot connection to a spring in series with a load cell and to a linear potentiometer in parallel to the spring and load cell (*c*).

moments were applied by reversing the sensor in the rigid fixture. The same tests were performed loading the sensor with known moments in the frontal plane to test sensitivity to off-axis loading. Maximum error from coupling of sagittal and frontal plane moments within normal walking load range was calculated. Known axial loads were applied as well ranging from 0 to 1000 N, recording sensor output voltages. The data were fit with linear regression lines and standard errors were calculated. Combined loading was not performed due to limited capability of applying known combined loads, i.e., if axial compression is applied with a known moment, it would not be possible to differentiate between off-axis loading contributing to sensor response and coupling between axial and moment loading.

Initial tuning for closed-loop moment control required constraining the prosthesis linkage from movement during actuation such that a moment was present at the proximal end where the moment sensor was located but not at the distal end of the prosthesis. This was to prevent the test setup from being overconstrained. A rigid fixture was bolted to the moment sensor and pinned at the lower posterior link (Fig. 6(*b*)). In this configuration, a moment could be generated at the sensor that was a product of reaction forces at the pin, accounting for all of the forces in the system. The pinned link had multiple positions at (1%, 33%, 66%, and 99% extension) so that performance could be verified through the entire range of motion. Due to spatial constraints on the rigid fixture, smaller extension increments would have required multiple testing fixtures introducing testing inconsistencies and were omitted. Using Ziegler–Nichols tuning method, a PID force controller was tuned for a moment step of 40 N · m. Prosthesis response at all fixed positions were recorded.

After initial tuning, response to maximum current step command was demonstrated in the same rigid fixture used for tuning (Fig. 6(*b*)). The prosthesis was commanded the maximum current of 15 A, and data were recorded for ten trials at each of four positions throughout the range of motion. Due to the constraints of the rigid fixture, no moment was present at the pinned end of the prosthesis and all the forces between the prosthesis and fixture were accounted for, assuming that frictional forces from small movements were negligible.

The frequency response throughout the range of motion of the prosthesis was obtained with the prosthesis mounted in the same rigid fixture used for tuning and maximum force step responses. In this test, the force controller tracked a chirp reference with feedback from the moment sensor to demonstrate closed-loop force control bandwidth. The chirp signal command had an amplitude of 10 N · m and offset by 15 N · m so that loading was always positive, as demonstrated in Ref. [29], sweeping from 0 to 30 Hz over 120 s. The test was performed ten times at each position. Data from individual trials were postprocessed, calculating cross power spectral density for amplitude response and phase shift. Data were then averaged over the ten trials for each position.

The power output of the prosthesis was evaluated by using a different characterization fixture, designed to act as a dynamometer. The fixture kept the mechanism fixed rigidly at the moment sensor and had tension springs at the foot attachment end to provide resistance during plantar flexion (Fig. 6(*c*)). Spring values were chosen to ensure that the motor would operate within its normal operating velocity range, and so the current controller, which was optimized for slower motor speeds at higher currents, could track the given command. The springs were attached to a uniaxial load cell (Omega, lc-202) in series to measure tension, and the load cell was attached to a pinned joint allowing only tension to be measured. A precision linear potentiometer (Omega, LP804-6) was attached parallel to the springs to measure spring deflection and estimate velocity during extension. The prosthesis was given a maximum step command of 15 A for 0.5 s to measure velocity and force output for power calculations. The current was then dropped to 7.5 A, followed by a ramp of −1.0 A/s to unload the dynamometer without damage occurring to hardware components.

2.4 Active Alignment Evaluation. Active alignment for the ankle–foot prosthesis was evaluated with an able-bodied subject, prior to future testing with subjects with lower limb amputation. Able-bodied adapters were fabricated to allow a subject without amputation to walk on the prosthesis for both controller development and demonstration of active alignment (Fig. 7). The test subject was male, 30 yrs of age with height and weight of 1.67 m and 69.7 kg, respectively. Testing took place in a lab setting and consisted of treadmill walking at a constant speed of 1.0 m/s. During

Fig. 7 Experimental prosthesis able-bodied adapters allow a person without amputation to walk on the prosthesis for preliminary testing. The contralateral limb is attached to a pylon and matching passive ESAR foot prosthesis aligned to match the neutral (retracted) position of the experimental prosthesis. The use of adapters accelerates the controller development and tuning without the need for test subjects with amputation.

testing, an overhead safety harness with a locking mechanism was used, as well as parallel bars alongside the treadmill for safety. The magnitude of the socket interface moment during walking was compared between active alignment tests and neutral alignment tests.

An initial walking controller was developed and implemented for early evaluation. A finite state machine monitored data from prosthesis sensors in real time to regulate gains and references used by a position controller throughout all the phases of walking (Fig. 8), similar to Ref. [30]. The finite state machine divided walking into three phases: early stance, mid-to-late stance, and swing, only allowing forward progression through gait when transition events were detected. The transition events consisted of HS, foot flat (FF), and TO, each triggering updates for controller gains and reference targets used by the position controller based on the walking state, cadence, and stance time. Events were detected when moment (M), moment derivative (dM), and angular acceleration (α) of the residual limb exceeded threshold combinations based on recorded walking data when the prosthesis was regulated at the neutral position. For ease of laboratory testing, the controller was automatically activated if mid-to-late stance time is less than 0.7 s for four consecutive steps. Once active, the controller automatically deactivated if late stance time exceeds 1.0 s in order to avoid unwanted deactivation when slowly changing walking speeds.

During early stance from HS to FF (measured global shank angle of zero), a low gain position controller held the foot at a neutral alignment. This prevented extension due to negative moment upon HS. At FF, the gains were increased as the position controller tracked a moving reference. The moving alignment reference, ψ^k, for step k had a derivative, $(d\psi^k/dt)$, that equaled the target alignment, ψ_{target} (desired maximum extension percent for the current step k), divided by the previous step stance time, t^{k-1}_{stance}, multiplied by an alignment coefficient, $\lambda_{\text{alignment}}$, as shown in Eq. (5). The alignment coefficient, $\lambda_{\text{alignment}}$, is the inverse of the intended percent of stance that alignment was to occur. By integrating Eq. (5), we attained the moving alignment reference, ψ^k_n, in Eq. (6) for sample n during stance. For initial testing, $\lambda_{\text{alignment}}$ was set to 2 in order to ensure that the alignment occurred before push off in late stance and the target alignment used was 100% to demonstrate full actuation. When the target alignment was reached, the reference signal became constant until TO was detected. The swing state then gave a neutral position reference,

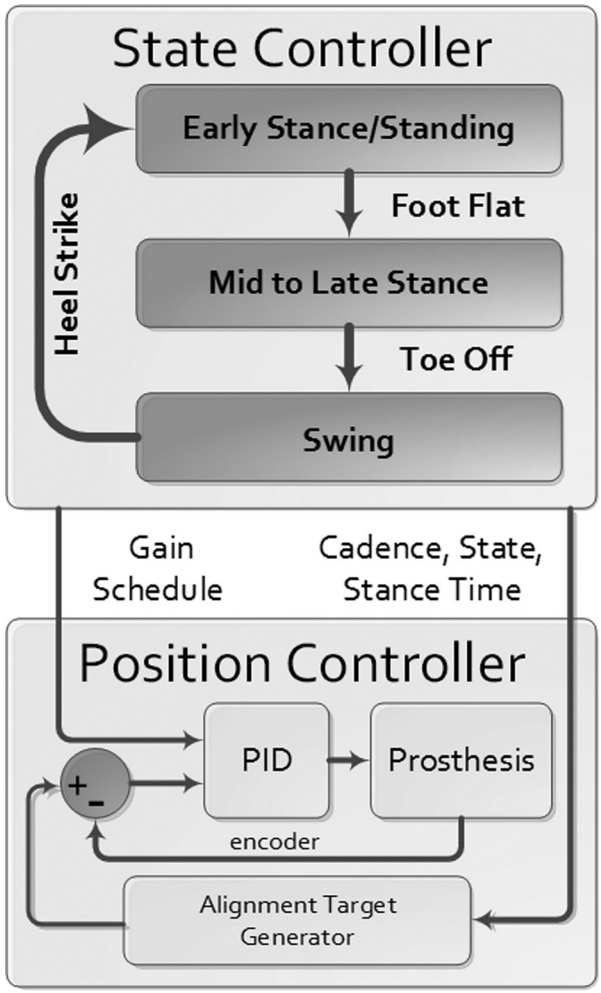

Fig. 8 Flow diagram of control methodology. A finite state controller is used to schedule gains for a PID position controller for each state. A reference target is calculated for each state based on cadence, state, and the stance time of the previous step.

and the prosthesis quickly retracted to a neutral position for swing phase foot clearance. With this method, the reference target velocity during stance was a function of walking speed, and the controller quickly adapted to different cadences

$$\frac{d\psi^k}{dt} = \lambda_{\text{alignment}} \frac{\psi^k_{\text{target}}}{t^{k-1}_{\text{stance}}} \tag{5}$$

$$\psi^k_n = \psi^k_{n-1} + \int \lambda_{\text{alignment}} \frac{\psi^k_{\text{target}}}{t^{k-1}_{\text{stance}}} dt \tag{6}$$

To demonstrate active alignment, able-bodied adapters adapted from Ref. [31] and shown in Fig. 7 were fabricated to allow a person without amputation to walk on the active alignment prosthesis. The adapters were fabricated from modified roller blades (Roller Derby Proline 900) bolted to AA6061 plates and standard off-the-shelf pyramid connectors. One adapter was attached to the active alignment prosthesis, and the contralateral adapter was attached to an uninstrumented pylon and matching passive ESAR foot. During treadmill walking at a constant speed of 1.0 m/s, sensor data were collected for ten steps when implementing active alignment mode and ten steps when regulating the static neutral alignment throughout stance. During postprocessing, recorded data were smoothed with a moving average filter with a ten sample window to remove artifacts and high-frequency noise,

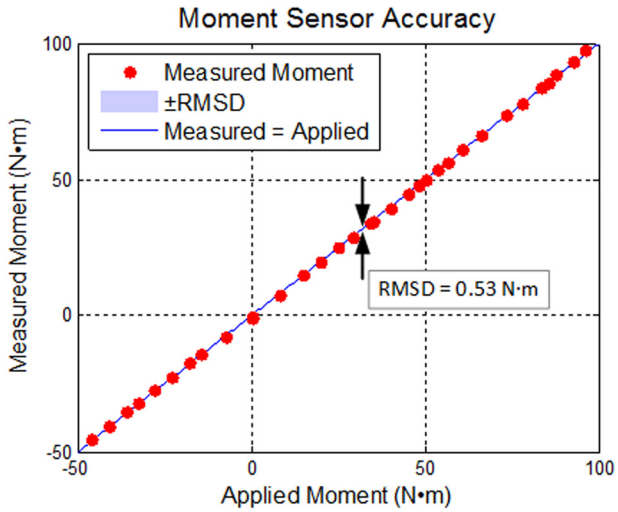

Fig. 9 Moment sensor accuracy showing the known applied moment in comparison to the moment recorded by the moment sensor and the RMS deviation as a shaded region

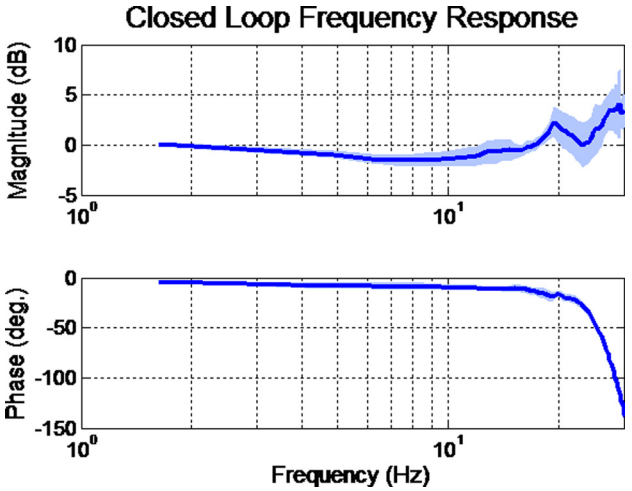

Fig. 11 Closed-loop force control frequency response of the prosthesis extended 66%. Fixed in a bench top characterization apparatus, the system was very stiff and did not display magnitude cutoff. The prosthesis was observed to be controllable up to about 20 Hz. Shortly after resonating at about 20 Hz, the response exhibited higher modalities and became unstable. Responses in all the amounts of extension were similar, having standard deviations that overlapped with the response shown.

normalized to body mass, resampled to normalize time to percentage of stance and averaged over the ten steps. Initial testing did not include full body biomechanics data.

3 Results

The active alignment prosthesis is an experimental prosthesis built to explore the benefits of altering residual limb kinematics to reduce loading demands, rather than merely mimicking physiological form and function of the lost limb. The experimental prosthesis is 18.4 cm tall and weighs 1.9 kg as tested, including the foot shell. During extension, the foot rotates 10 deg and translates 54.7 mm posteriorly and 22.7 mm distally. Link lengths and attachment angles are shown in Fig. 4.

The socket moment sensor was tested and calibrated for a range of −50 to 100 N · m (Fig. 9). The sensor produced a mean of 25.5 mV/N · m applied. All the measurement errors were less than 1.55 N · m, and the rms deviation was 0.53 N · m with pure sagittal moment loading. Off-axis frontal plane moment loading showed a sensitivity of 0.22 mV/N · m, and direct axial loading was not measurable due to uncertainty of whether the axial loads were perfectly perpendicular to the sensor. Calculated coupling of sagittal and frontal plane moments produced a maximum error of 2.1% with normal frontal moment loading during gait.

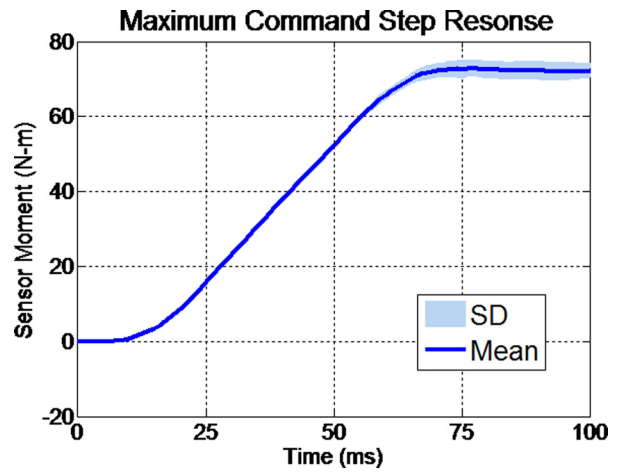

Fig. 10 Moment generated at the moment sensor of the prosthesis when fixed extended 66% in a bench top jig and commanded a maximum current to the motor. Average rise times at all the positions were less than 60 ms for 90% final value, having standard deviations that overlapped.

Step responses to maximum current command were recorded to examine moment response times. The prosthesis was constrained from movement in four extension positions having different mechanical advantage for ten trials each. Extension positions were 0%, 33%, 66%, and 99%. Peak moment rise times were no more than 60 ms for 90% of the maximum recorded value in all the trials. Response when fixed at 66% extension can be seen in Fig. 10.

The frequency response was evaluated at the same extension percentages of prosthesis travel. In all the positions, the prosthesis resonated at 20 Hz and entered into higher modal frequencies above 22 Hz. Although the standard bandwidth cutoff of −3 dB in magnitude was never seen, the phase shifted rapidly as it became unstable and entered higher modes of vibration. The maximum controllable frequency was measured at 20 Hz for all the positions. Figure 11 shows the frequency response of the prosthesis extended to 66% with standard deviation that overlaps with the response at all other extension amounts.

Peak mechanical power output of the prosthesis was measured to be 511 (±11.3) W, mean and standard deviation. The dynamometer was driven to a linear velocity of 1.10 (±0.02) m/s and measured 460 (±2.65) N at peak power for a mechanical efficiency of 85%. Motor current was saturated at the time of peak power.

Walking test results are shown in Fig. 12. The plot shows the sagittal plane moment recorded from the moment sensor during the stance phase of walking, normalized to body mass, when walking at a constant velocity of 1.0 m/s. The dashed line presents the average and standard deviation of the moments from ten steps when the prosthesis regulated at a neutral position, emulating a passive prosthesis. The solid line presents the average and standard deviation of the moments from ten steps recorded when implementing active alignment. Average peak moments for regulated neutral alignment and active alignment were calculated to be 1.22 ± 0.09 N · m/kg and 0.81 ± 0.06 N · m/kg, respectively. The results show that the peak moment during late stance was reduced by 33.6% on average when active alignment was implemented.

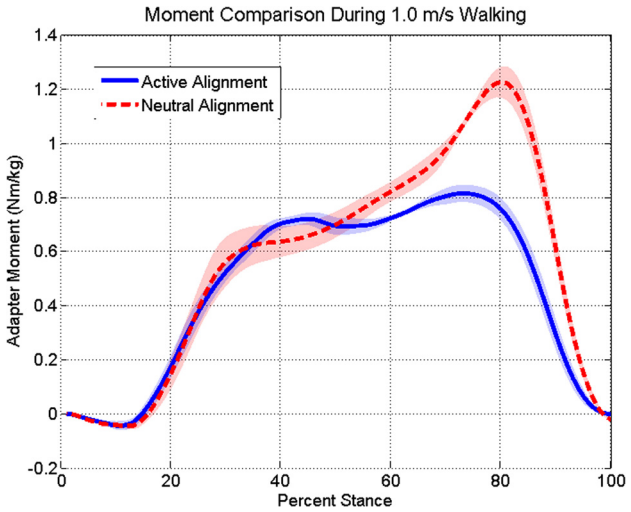

Fig. 12 Comparison of moments recorded by the prosthesis moment sensor while walking on a treadmill at a constant speed of 1.0 m/s while the prosthesis is regulating at a neutral alignment and actively aligning. The lines are averaged values for ten consecutive steps, and the shaded areas are standard deviations. The recorded data show a peak moment reduction of 33% during active alignment.

4 Discussion

An experimental prosthesis has been developed to evaluate active alignment in a lab setting. Active alignment shifts the residual limb anteriorly in relation to the foot and CoP during midstance. The prosthesis reduces the effective moment arm between the GRF and residual limb, while retaining energy storage and release in the foot prosthesis, as well as push off capabilities of an active prosthesis. Peak moment transfer at the socket interface during push off is reduced which is commonly associated with peak socket pressure. The device as developed is experimental and meant only for evaluation of the approach during level ground walking, in order to determine concept validity and feasibility. For this initial study, other activities of daily living are not addressed. Preliminary walking tests reveal that the moment is substantially reduced when active alignment is implemented in comparison to equivalent tests of neutral prosthesis alignment. These results suggest that implementing the novel functionality of active alignment into future transtibial prosthesis designs may lead to a more comfortable gait for persons with amputation, which could lead to increased mobility and enhanced quality of life.

The experimental ankle prosthesis is based on a four-bar linkage which rotates the foot while translating the foot center of rotation in the shank reference frame for active alignment. There are other mechanisms that can achieve active alignment, such as multiple degrees-of-freedom prismatic joints in series; however, this linkage was chosen for simplicity and it needs only a single actuator. The four-bar linkage also acts as a variable ratio transmission. The mechanical advantage of the device increases while the linear actuator pulls the anterior and posterior link joints closer in proximity. This increases the end effector to linear actuator force ratio as the prosthesis extends. In late stance, a greater linkage force is needed to overcome the larger reaction moment generated in the foot. The variable ratio feature is advantageous, as it enables more force to be generated by the actuator as the demand increases.

The link lengths and attachment angles of the prosthesis linkage are optimized based on able-bodied walking biomechanics and simulations of corrected biomechanics when a limb is missing. The constraints chosen to design the linkage were based on the assumption that active alignment can restore biomechanics (joint forces and trajectories) to near-normal values in the rest of the unaffected body, starting at one joint removed from amputation. It must be noted that the design constraints and modeling assumptions used are ideal. They are considered to be initial design criteria made in order to realize a new paradigm of prosthesis design, with the understanding that future work may require us to refine our approach. Future constraints will be based on findings from biomechanics analysis of gait while persons with amputation use the prosthesis prototype, testing validity of the assumptions.

The linkage is driven by a high power motor coupled to a pulley transmission and ball screw. Characterizations of performance were completed on the actuator and custom moment sensor. The moment sensor is seen to have a high linearity and repeatability having an rms deviation of $0.53\,\mathrm{N\cdot m}$ between measured and actual applied moments when applying and releasing loads ranging from $-50\,\mathrm{N\cdot m}$ to $100\,\mathrm{N\cdot m}$. This is within the range that is normally observed during normal walking for an able-bodied person having up to 83 kg of body mass. In order to accommodate larger persons, a redesign would be required of the pulley transmission with a higher reduction ratio. The linkage acting as a variable ratio transmission is observed to be advantageous due to the increase in moment demand as stance progresses during walking. This has the potential to allow smaller motors to be used assuming that the control strategy times the alignment to begin when loading demand is low. The prosthesis was found to be controllable up to 20 Hz throughout the entire range of motion demonstrating adequate bandwidth for normal walking speeds where cyclic loading is normally observed to be an order of magnitude less.

Preliminary tests performed to emulate gait of individuals with amputation utilized able-bodied adapters, which effectively elongated the shank. The tests reveal that the peak sagittal moment generated is on average 33% lower with active alignment in comparison to neutral aligned walking tests. It is also seen that after FF, when the prosthesis is actuating, the moment is slightly higher than normal (Fig. 12). This may be a result of positive work performed by the prosthesis during that time, however, work was not evaluated in this study. There are many unknowns about walking stability and the true dynamic interaction of the device and residual limb that may be clarified in future work including full body biomechanical analyses on persons with amputation. However, while observing an able-bodied subject walk with adapters there was no noticeable instability throughout gait, including when the device actuated during single-supported stance and retracted following TO. Although complete biomechanics analyses were not performed during preliminary testing, the gait did appear reasonably normal despite the extended shanks. The test subject was able to adapt very quickly to both the prosthesis adapters and the active alignment. The subject also reported that they were easy to walk on. Future biomechanics studies involving test subjects with amputation will examine CoM trajectory, work performed by the contralateral limb, net-positive work generated by the prosthesis, and subject metabolic cost.

The preliminary prototype is heavy, weighing 1.9 kg; however, the focus of this prototype is to study the effects active alignment has during walking in a lab setting. Future iterations of the device will need to be lighter and could show more promise in reducing metabolic cost and compensation by the rest of body. The moment sensor only accounts for a portion of the dynamics and does not provide insight to the linear force components being transferred or CoP. A multiaxis load cell or pressure sensors in the prosthesis heel and toe would give insight to the CoP and effective moment arm in real time. This would allow for more sophisticated control approaches that rely on complete dynamics being known and used for feedback. Additional future improvements will include a more compact design, improved cosmetics, a dedicated embedded system with a battery pack, and control methodologies that allow different activities throughout the day in a normal setting.

Although initial walking tests performed by a subject with intact limbs appear to be successful, it is unclear at this time how subjects with amputation will react to modified stance kinematics, and if there are limits to kinematic modifications that will be perceived as stable. This is mainly due to the limited knowledge of

the socket–limb kinetics. The assumption that only stance phase knee flexion will be modified may be false, and changes to the hip joint trajectories may also be modified if the person feels they need to better support themselves during the active limb alignment. It is anticipated that an adaptive controller which gradually increases the amount of alignment from step-to-step as a subject begins to walk will be beneficial and more intuitive to use. This will allow a more natural transition into an altered gait as the subject gains confidence in the modified mechanics.

5 Conclusion

In this paper, a tethered ankle prosthesis prototype was designed for evaluating active alignment during walking in a lab environment. Initial walking tests show a peak moment reduction of 33% at the prosthesis connection when active alignment is implemented, in comparison to neutral prosthesis alignment. These results demonstrate that active alignment may be implemented in powered lower limb prostheses to improve loading conditions for a more comfortable gait for persons with amputation.

Future work involves developing an improved adaptive control methodology to slowly increase the amount of realignment with each progressive step as a person gains confidence in the new device and modified gait mechanics. Full body biomechanical analysis on persons with amputation will follow for evaluation in a lab environment, giving insight to design requirements to be applied in future prosthesis designs realizing active alignment. Additionally, more work is needed to find optimal prosthesis kinematics and kinetics that can restore rest of body biomechanics with tolerable limb loads.

Acknowledgment

This work was supported in part by grants from the National Science Foundation (IIP-1439683 and IIS-1526986) and National Center for Simulation in Rehabilitation Research (NCSRR, Stanford University).

References

[1] Pitkin, M. R., 2010, *Biomechanics of Lower Limb Prosthetics*, Springer, Berlin.
[2] Norvell, D. C., Czerniecki, J. M., Reiber, G. E., Maynard, C., Pecoraro, J. A., and Weiss, N. S., 2005, "The Prevalence of Knee Pain and Symptomatic Knee Osteoarthritis Among Veteran Traumatic Amputees and Nonamputees," Arch. Phys. Med. Rehabil., **86**(3), pp. 487–493.
[3] Struyf, P. A., van Heugten, C. M., Hitters, M. W., and Smeets, R. J., 2009, "The Prevalence of Osteoarthritis of the Intact Hip and Knee Among Traumatic Leg Amputees," Arch. Phys. Med. Rehabil., **90**(3), pp. 440–446.
[4] Hammarlund, C. S., Carlström, M., Melchior, R., and Persson, B. M., 2011, "Prevalence of Back Pain, Its Effect on Functional Ability and Health-Related Quality of Life in Lower Limb Amputees Secondary to Trauma or Tumour: A Comparison Across Three Levels of Amputation," Prosthet. Orthot. Int., **35**(1), pp. 97–105.
[5] Gailey, R., Allen, K., Castles, J., Kucharik, J., and Roeder, M., 2008, "Review of Secondary Physical Conditions Associated With Lower-Limb Amputation and Long-Term Prosthesis Use," J. Rehabil. Res. Dev., **45**(1), pp. 15–29.
[6] Johnson, V. J., Kondziela, S., and Gottschalk, F., 1995, "Pre and Post-Amputation Mobility of Trans-Tibial Amputees: Correlation to Medical Problems, Age and Mortality," Prosthet. Orthot. Int., **19**(3), pp. 159–164.
[7] Au, S. K., and Herr, H. M., 2008, "Powered Ankle–Foot Prosthesis," IEEE Rob. Autom. Mag., **15**(3), pp. 52–59.
[8] Bergelin, B. J., and Voglewede, P. A., 2012, "Design of an Active Ankle–Foot Prosthesis Utilizing a Four-Bar Mechanism," ASME J. Mech. Des., **134**(6), p. 061004.
[9] Sun, J., and Voglewede, P. A., 2013, "Powered Transtibial Prosthetic Device Control System Design, Implementation, and Bench Testing," ASME J. Med. Devices, **8**(1), p. 011004.
[10] Zajac, F. E., Neptune, R. R., and Kautz, S. A., 2003, "Biomechanics and Muscle Coordination of Human Walking—Part II: Lessons From Dynamical Simulations and Clinical Implications," Gait Posture, **17**(1), pp. 1–17.
[11] Neptune, R. R., Zajac, F. E., and Kautz, S. A., 2004, "Muscle Force Redistributes Segmental Power for Body Progression During Walking," Gait Posture, **19**(2), pp. 194–205.
[12] Neptune, R. R., and McGowan, C. P., 2011, "Muscle Contributions to Whole-Body Sagittal Plane Angular Momentum During Walking," J. Biomech., **44**(1), pp. 6–12.
[13] Herr, H. M., and Grabowski, A. M., 2012, "Bionic Ankle–Foot Prosthesis Normalizes Walking Gait for Persons With Leg Amputation," Proc. R. Soc. B Biol. Sci., **279**(1728), pp. 457–464.
[14] D'Andrea, S., Wilhelm, N., Silverman, A. K., and Grabowski, A. M., 2014, "Does Use of a Powered Ankle–Foot Prosthesis Restore Whole-Body Angular Momentum During Walking at Different Speeds?" Clin. Orthop. Relat. Res., **472**(10), pp. 3044–3054.
[15] Radcliffe, C. W., and Foort, J., 1961, "The Patellar-Tendon-Bearing Below-Knee Prosthesis," Biomechanics Laboratory, University of California, Berkeley, CA.
[16] Kapp, S., and Cummings, D., 2002, *Atlas of Amputations and Limb Deficiencies: Surgical, Prosthetic, and Rehabilitation Principles; Transtibial Amputation: Prosthetic Management*, American Academy of Orthopedic Surgeons, Rosemont, IL.
[17] Jia, X., Zhang, M., and Lee, W. C. C., 2004, "Load Transfer Mechanics Between Trans-Tibial Prosthetic Socket and Residual Limb—Dynamic Effects," J. Biomech., **37**(9), pp. 1371–1377.
[18] Seelen, H. A. M., Anemaat, S., Janssen, H. M. H., and Deckers, J. H. M., 2003, "Effects of Prosthesis Alignment on Pressure Distribution at the Stump/Socket Interface in Transtibial Amputees During Unsupported Stance and Gait," Clin. Rehabil., **17**(7), pp. 787–796.
[19] Hachisuka, K., Dozono, K., Ogata, H., Ohmine, S., Shitama, H., and Shinkoda, K., 1998, "Total Surface Bearing Below-Knee Prosthesis: Advantages, Disadvantages, and Clinical Implications," Arch. Phys. Med. Rehabil., **79**(7), pp. 783–789.
[20] Selles, R. W., Janssens, P. J., Jongenengel, C. D., and Bussmann, J. B., 2005, "A Randomized Controlled Trial Comparing Functional Outcome and Cost Efficiency of a Total Surface-Bearing Socket Versus a Conventional Patellar Tendon-Bearing Socket in Transtibial Amputees," Arch. Phys. Med. Rehabil., **86**(1), pp. 154–161.
[21] Henrot, P., Stines, J., Walter, F., Martinet, N., Paysant, J., and Blum, A., 2000, "Imaging of the Painful Lower Limb Stump," Radiographics, **20**, pp. S219–S235.
[22] Boone, D. A., Kobayashi, T., Chou, T. G., Arabian, A. K., Coleman, K. L., Orendurff, M. S., and Zhang, M., 2013, "Influence of Malalignment on Socket Reaction Moments During Gait in Amputees With Transtibial Prostheses," Gait Posture, **37**(4), pp. 620–626.
[23] Hatfield, A. G., and Morrison, J. D., 2001, "Polyurethane Gel Liner Usage in the Oxford Prosthetic Service," Prosthet. Orthot. Int., **25**(1), pp. 41–46.
[24] Boutwell, E., Stine, R., Hansen, A., Tucker, K., and Gard, S., 2012, "Effect of Prosthetic Gel Liner Thickness on Gait Biomechanics and Pressure Distribution Within the Transtibial Socket," J. Rehabil. Res. Dev., **49**(2), pp. 227–240.
[25] LaPre, A. K., Umberger, B. R., and Sup, F., 2014, "Simulation of a Powered Ankle Prosthesis With Dynamic Joint Alignment," 36th Annual International Conference on Engineering in Medicine and Biology Society (EMBC), Chicago, IL, Aug. 26–30, pp. 1618–1621.
[26] LaPre, A. K., and Sup, F., 2013, "Redefining Prosthetic Ankle Mechanics: Non-Anthropomorphic Ankle Design," IEEE International Conference on Rehabilitation Robotics (ICORR), Seattle, WA, June 24–26.
[27] Sup, F., Bohara, A., and Goldfarb, M., 2008, "Design and Control of a Powered Transfemoral Prosthesis," Int. J. Rob. Res., **27**(2), pp. 263–273.
[28] Hang, C. C., Åstroüm, K. J., and Ho, W. K., 1991, "Refinements of the Ziegler–Nichols Tuning Formula," IEEE Proc. D Control Theory Appl., **138**(2), pp. 111–118.
[29] Caputo, J. M., and Collins, S. H., 2014, "A Universal Ankle–Foot Prosthesis Emulator for Human Locomotion Experiments," ASME J. Biomech. Eng., **136**(3), p. 035002.
[30] Varol, H. A., Sup, F., and Goldfarb, M., 2010, "Multiclass Real-Time Intent Recognition of a Powered Lower Limb Prosthesis," IEEE Trans. Biomed. Eng., **57**(3), pp. 542–551.
[31] Shultz, A. H., Mitchell, J. E., Truex, D., Lawson, B. E., and Goldfarb, M., 2013, "Preliminary Evaluation of a Walking Controller for a Powered Ankle Prosthesis," IEEE International Conference on Robotics and Automation (ICRA), Karlsruhe, Germany, May 6–10, pp. 4837–4843.